BRIEF COMMUNICATIONS

Parvalbumin interneurons mediate neuronal circuitry-neurogenesis coupling in the adult hippocampus

Juan Song, Jiaqi Sun, Jonathan Moss, Zhexing Wen, Gerald J. Sun, Derek Hsu, Chun Zhong, Heydar Davoudi, Kimberly M. Christian, Nicolas Toni, Guo-li Ming and Hongjun Song

Summary of supplementary information:

Supplementary Figs. 1-9

Supplementary Movies 1-2

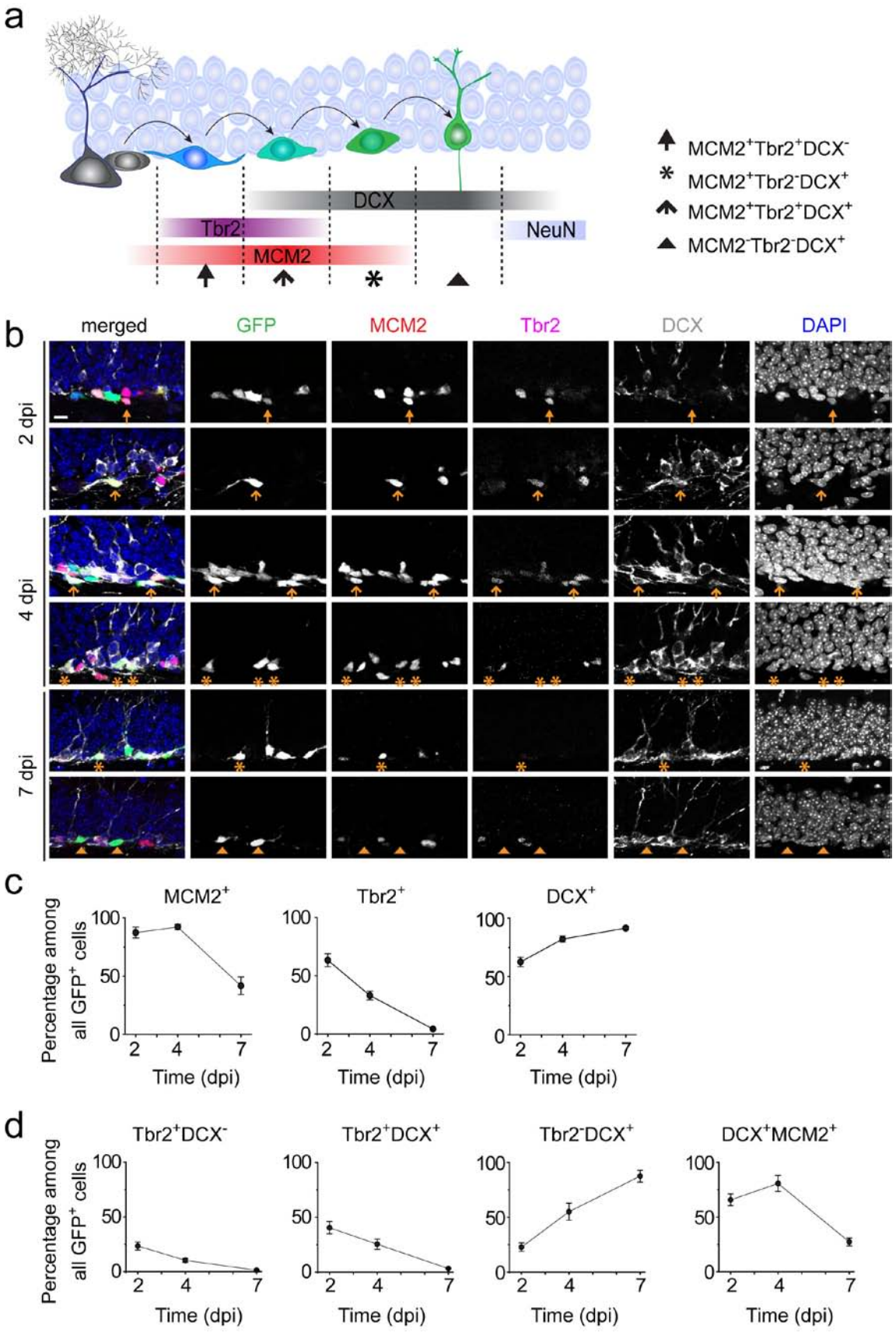

Supplementary Fig. 1. Immunohistological characterization of newborn progeny during early proliferative phases of adult hippocampal neurogenesis. (**a**) A schematic diagram of the current view of progenitor subtypes and their marker expression during early phases of adult

hippocampal neurogenesis. (**b-d**) Time course analysis of marker expression by retrovirally-labelled precursors in the adult dentate gyrus. Engineered onco-retroviruses expressing GFP were stereotaxcially injected into the adult mouse dentate gyrus. Shown in (**b**) are sample confocal images of staining for GFP, MCM2, Tbr2, DCX and DAPI. Scale bar: 10 μm. Shown in (**c-d**) are quantifications of different precursor subtypes among all GFP^+ cells at 2, 4 and 7 days post injection (dpi). Values represent mean ± s.e.m. (n = 3-5 animals).

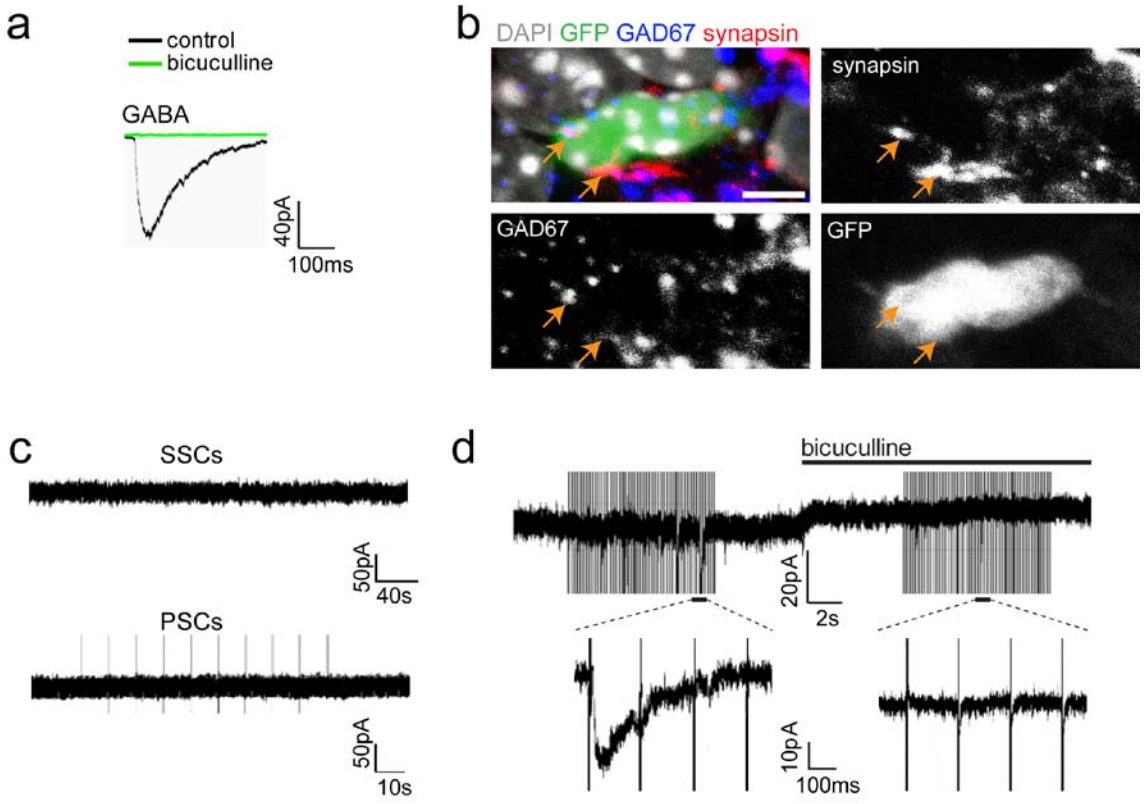

Supplementary Fig. 2. Electrophysiological characterization of newborn progeny during early proliferative phases of adult hippocampal neurogenesis. (**a**) Sample whole-cell voltage-clamp (V_m = -65 mV) recording traces of a GFP^+ cell in the slice acutely prepared from injected animals at 4 dpi in response to puff of GABA (10 μM) in the presence or absence of bicuculline (100 μM). (**b**) Sample confocal images of staining of GFP, synapsin I (a synaptic vesicle protein), GAD67 (a GABAergic neuron marker), and DAPI. Scale bar: 5 μm. Arrows point to $GAD67^+synapsin^+$ puncta. Please see **Supplementary Movie 1** for 3D reconstruction and detail. (**c**) Sample whole-cell voltage-clamp recording traces from a GFP^+ cell in the slice acutely prepared from injected animals at 4 dpi. Note a lack of spontaneous synaptic current (SSC) and evoked postsynaptic current (PSC) in response to low frequency field stimulation (0.1 Hz) of the dentate granule cell layer. (**d**) Sample whole-cell voltage-clamp recording traces of a GFP^+ cell at 4 dpi in the acute slice in response to 5 Hz stimulation of dentate granule cell layer in the absence and presence of bicuculline (100 μM).

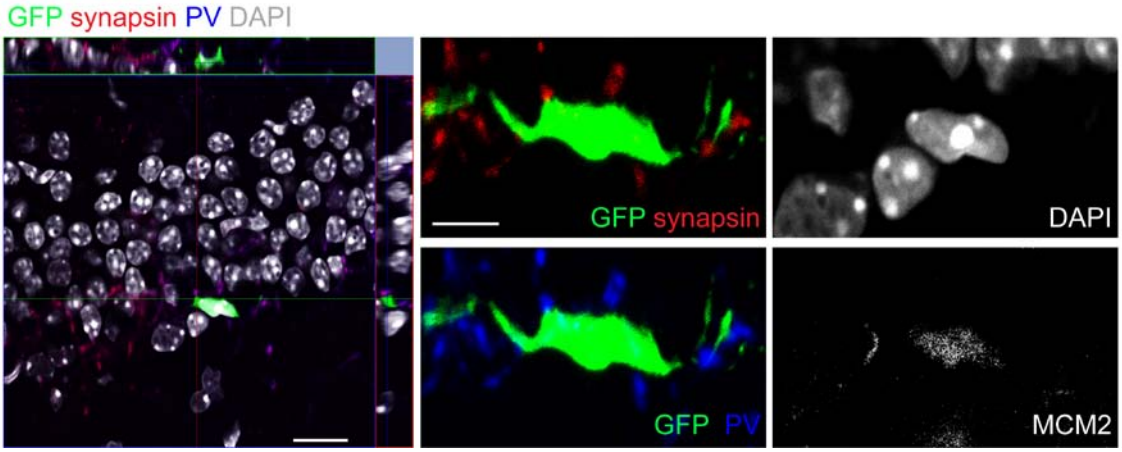

Supplementary Fig. 3. Synaptic inputs onto proliferating neural progeny from PV^+ interneurons. Shown are sample confocal images of GFP^+ newborn progeny at 4 dpi with immunostaining of synapsin, PV and a proliferation marker MCM2, and DAPI. Scale bars: 20 μm (left panel) and 10 μm (right two panels).

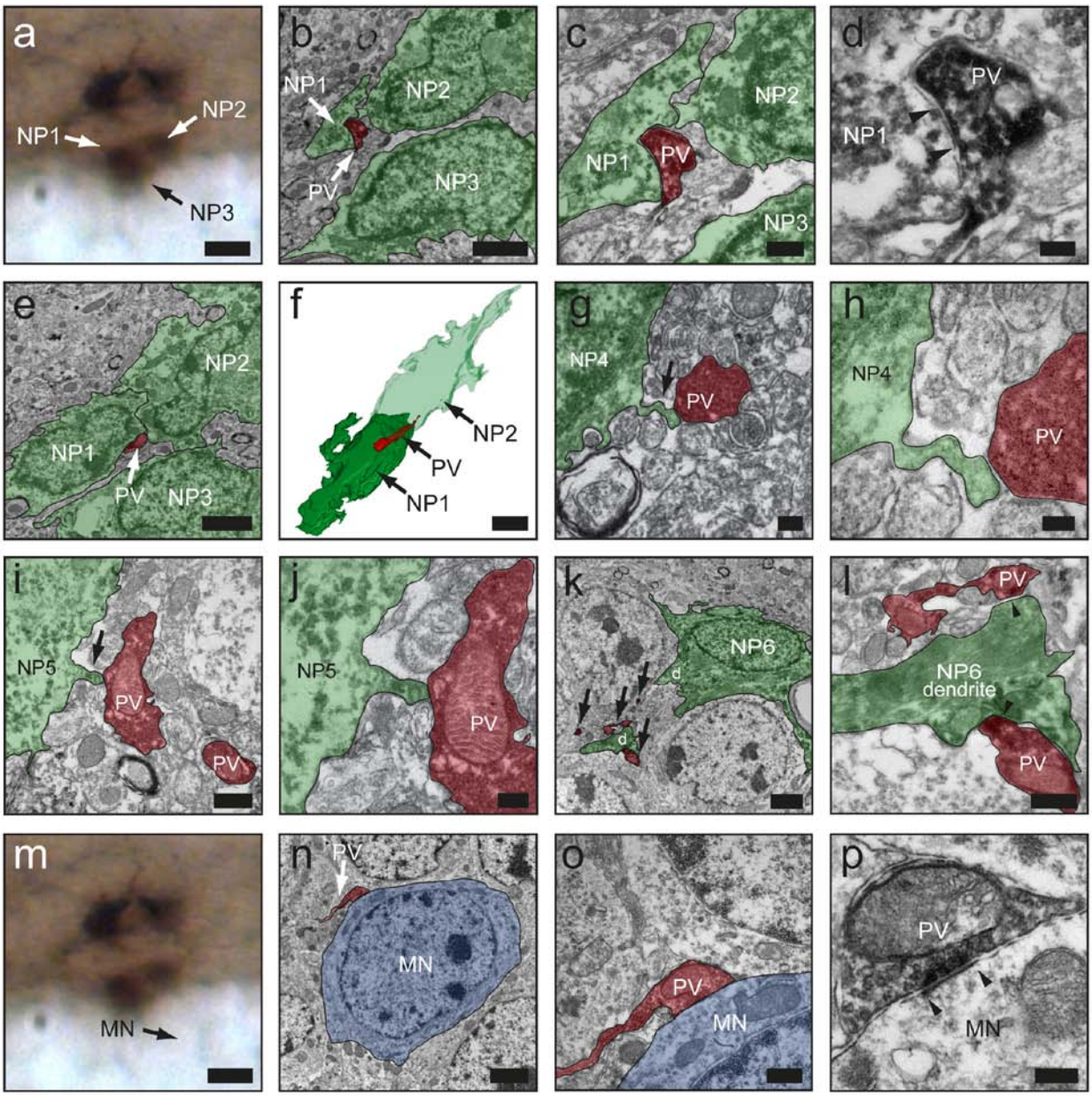

Supplementary Fig. 4. Immuno-EM analyses of synapses and close appositions between PV^+ axon terminals and newborn progeny in the adult dentate gyrus. Shown in (**a-f**) are steps to identify synaptic contact between a labelled PV^+ axon terminal and labelled newborn progeny as shown in **Fig. 1c**. Locations of the newborn progeny (NP) were identified at the light microscopic level (**a**) and followed through to the electron microscopic level (**b-f**). Electron micrographs at increasing magnifications (**b-d**) show the position of the PV^+ axon terminal in relation to three of the newborn progeny (NPs 1-3). The high magnification view of the PV^+ axon terminal forming a symmetrical synaptic contact (arrowheads) with the labelled newborn progeny is shown in (**d**) and **Fig. 1c**. The morphology of the NP1 cell body is lacking from (**b-d**), but is shown in (**e**) with the PV^+ axon closely apposed. To further describe the relationship between the PV^+ axon and NPs 1 and 2, they have been reconstructed in 3D shown in (**f**). Various contacts between PV^+ axons and newborn progeny in the adult dentate gyrus are shown in (**g-l**). Shown in (**g-j**) are two examples of PV^+ axons closely apposing the tips of filopodia extending from labelled newborn progeny (NPs 4 and 5), at low and high magnifications. Shown in (**k-l**), PV^+ axon segments (arrows in **k**) are seen both in the vicinity of a labelled newborn progeny (NP6) and closely apposing its principal dendritic extension (arrowheads in **l**). Note also the presence of

cytoskeleton fibers within the dendritic extension of the newborn progeny. Shown in (**m-p**) are processes to identify synaptic contact between a labelled PV^+ axonal terminal and an unlabelled mature granule neuron (MN) as shown in **Fig. 1e**. The location of the mature neuron (arrow) was identified at the light microscopic level (**m**) and followed through to the electron microscopic level (**n-p**). Electron micrographs at increasing magnifications (**n-p**) show the position of the PV^+ axon terminal in relation to the mature neuron. The high magnification view of the PV^+ axon terminal forming a symmetrical synaptic contact (arrowheads) with the mature neuron is shown in (**p**) and **Fig. 1e**. Newborn progeny are coloured in green, PV^+ axons in red and mature granule neurons in blue. Scale bars: **a**, 10 µm; **b**, 2 µm; **c**, 0.5 µm; **d**, 0.2 µm; **e**, 2 µm; **f**, 2 µm; **g**, 0.2 µm; **h**, 0.1 µm; **i**, 0.5 µm; **j**, 0.2 µm; **k**, 2 µm; **l**, 0.5 µm; **m**, 10 µm; **n**, 2 µm; **o**, 1 µm; **p**, 0.2 µm.

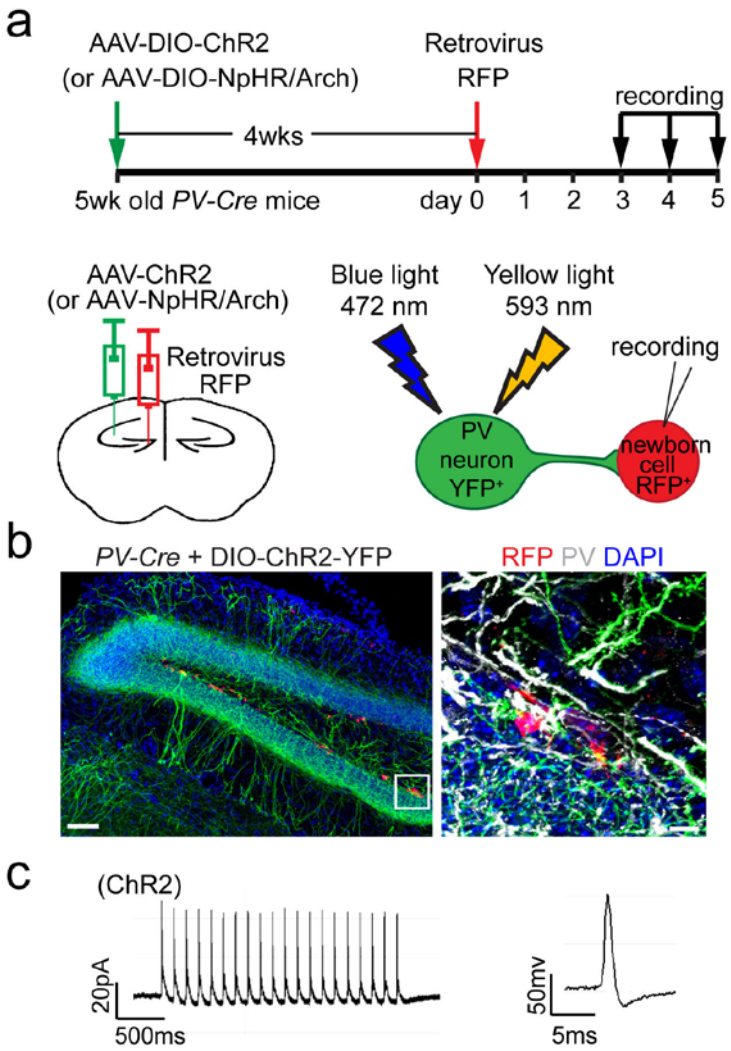

Supplementary Fig. 5. Characterization of PV$^+$ neuron synaptic inputs onto newborn progeny with optogenetic tools. (**a-b**) Targeting of PV$^+$ neurons and newborn progeny with engineered AAV and onco-retrovirus, respectively. Shown in (**a**) is a schematic diagram of the experimental design. Engineered AAV with Cre-dependent expression of ChR2-YFP, NpHR-YFP or Arch-YFP was stereotaxically injected into the dentate gyrus of 5 week-old *PV-Cre* mice and retrovirus expressing RFP was stereotaxically injected 4 weeks later. Electrophysiological recordings of RFP$^+$ cells were carried out in slices acutely prepared from injected animals at 3-5 dpi. Shown in (**b**) are sample confocal images of ChR2-YFP and RFP in the dentate gyrus from AAV and retroviral injected *PV-Cre* animals. Note the wide spread of YFP$^+$ fibers surrounding RFP$^+$ cells. Scale bars: 50 μm (left) and 10 μm (right). (**c**) Effective light-induced manipulation of PV$^+$ neuron firing in slices acutely prepared from AAV injected animals. Shown are sample traces of whole-cell recording of a ChR2-YFP$^+$ neuron under current-clamp mode upon light-stimulation (472 nm blue light at 8 Hz, 5 ms).

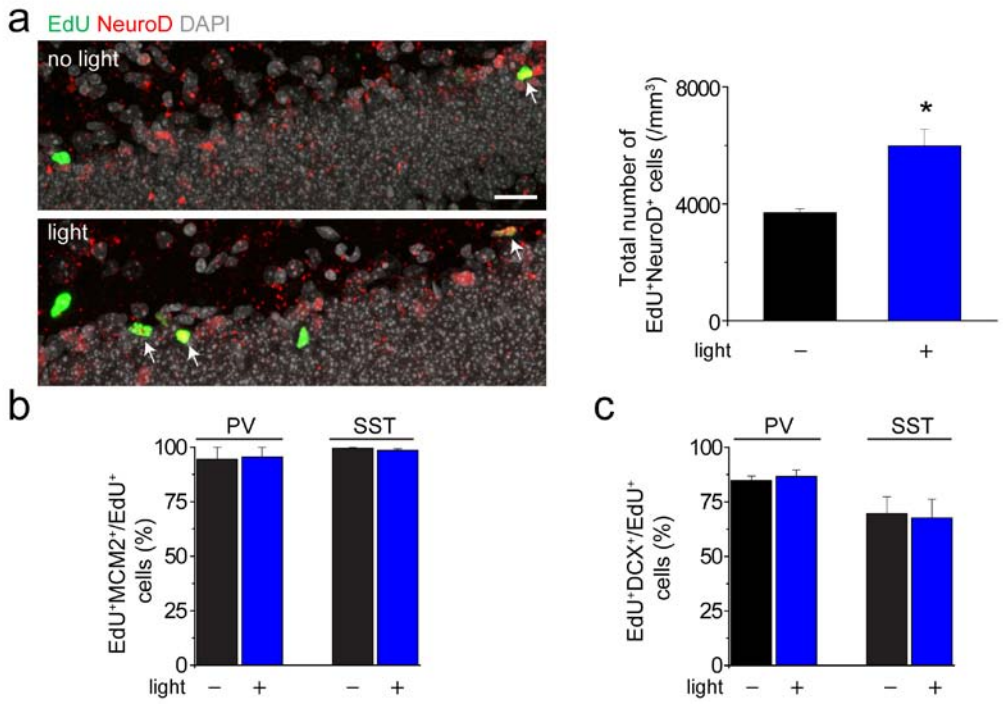

Supplementary Fig. 6. Effect of optogenetic activation of PV^+ or SST^+ interneurons during early proliferative phases of adult hippocampal neurogenesis *in vivo*. (**a**) Increased $NeuroD^+$ newborn progeny upon PV^+ neurons activation. Shown on the left are sample confocal images of of NeuroD immunostaining, EdU and DAPI. Arrows point to $EdU^+NeuroD^+$ newborn progeny. Scale bar: 50 μm. Shown on the right is a summary of quantification of $EdU^+NeuroD^+$ cells under different conditions. Values represent mean ± s.e.m. (n = 3 animals; *: $P < 0.05$; Student's t-test). (**b-c**) Quantifications of percentages of EdU^+ cells that were also $MCM2^+$ (proliferating neural progeny; **b**), or were DCX^+ (newborn neuronal progeny; **c**) at 4 dpi. Values represent mean ± s.e.m. (n = 3-5 animals; $P > 0.10$; Student's t-test). The same groups of animals as in **Figs. 2c-d** were examined.

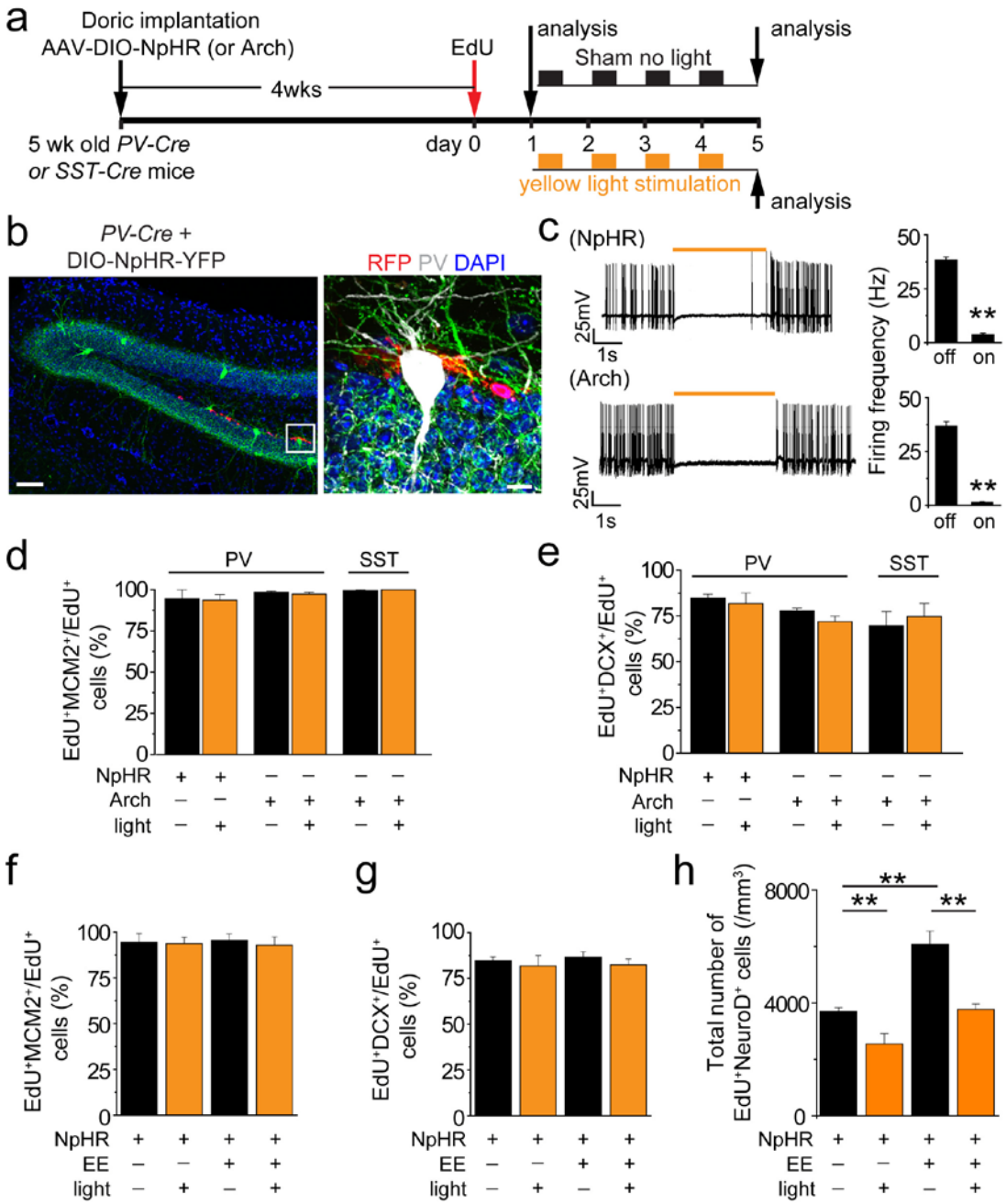

Supplementary Fig. 7. Effect of suppressing PV^+, or SST^+, interneuron activation during early phases of adult hippocampal neurogenesis *in vivo*. (**a**) A schematic diagram of experimental design for **Fig. 3a-e**. EdU (41.1 mg/kg body weight) was *i.p.* injected 4 times 2.5 hrs apart at day 0 and continuous yellow light (593 nm; constant or no light sham control) was delivered 8 hrs per day between day 1 and day 4. Animals were processed for analysis on day 1 or day 4. (**b**) Sample confocal images of NpHR-YFP and RFP in the dentate gyrus from AAV and retroviral injected *PV-Cre* animals. Note the wide spread of YFP^+ fibers surrounding RFP^+ cells. Scale bars: 50 μm (left) and 10 μm (right). (**c**) Effective light-induced suppression of PV^+ neuron firing in slices acutely prepared from AAV injected animals. Shown are sample traces of whole-cell recordings of NpHR- or Arch-expressing YFP^+ neurons under current-clamp mode upon light stimulation (593 nm yellow light; constant). A current pulse of 100 pA current was delivered to YFP^+ neurons, and the number of action potentials was quantified with or without yellow light on. Values represent mean ± s.e.m. (n = 6 cells; **: $P < 0.01$; Student's t-test). (**d-e**) Quantification

of percentages of EdU^+ cells that were $MCM2^+$ (proliferating neural progeny; **d**), or were DCX^+ (newborn neuronal progeny; **e**) at 4 dpi. The same groups of animals as in **Figs. 3a-b** were examined. Values represent mean $\pm$ s.e.m. (n = 3-5 animals; $P > 0.10$; Student's t-test). (**f-h**) Quantification of percentages of EdU^+ cells that were $MCM2^+$ (proliferating neural progeny, **f**), or were DCX^+ (newborn neuronal progeny, **g**), and stereological quantification of $EdU^+NeuroD^+$ cells (**h**) at 4 dpi. The same groups of animals as in **Fig. 3h** were analyzed. Values represent mean $\pm$ s.e.m. (n = 3-5 animals; **: $P < 0.01$; two-way ANOVA).

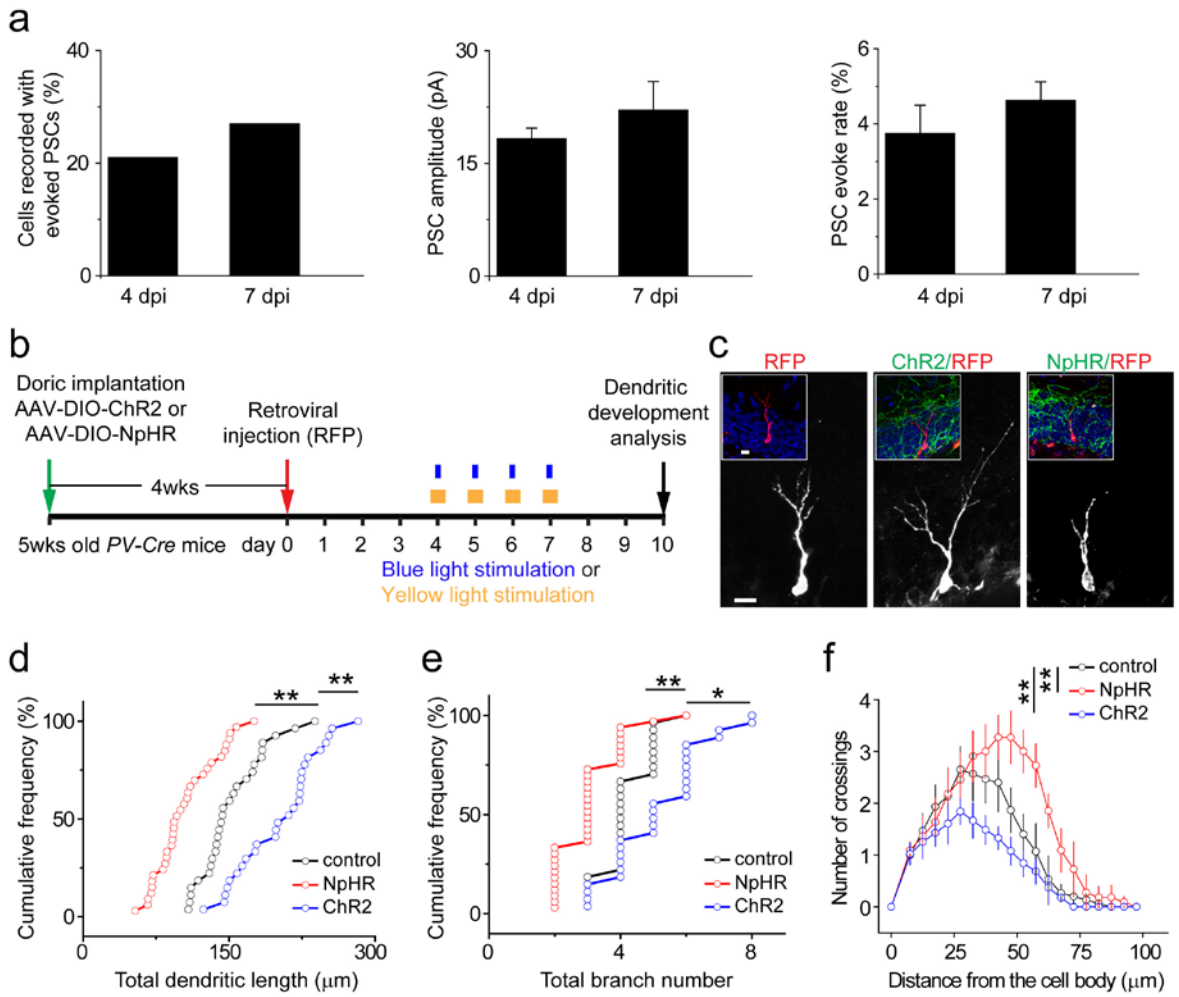

Supplementary Fig. 8. PV$^+$ neuron activity regulates dendritic growth of newborn neurons during adult hippocampal neurogenesis. (**a**) Presence of GABAergic synaptic inputs onto newborn neurons at 7 dpi from PV$^+$ neurons. Same as in **Fig. 1g**, except that GFP$^+$ newborn progeny at 4 and 7 dpi were examined and summaries for percentages of GFP$^+$ cells recorded that exhibited PSCs (left), the mean amplitudes of PSCs (middle) and the PSC induction rate (right) are shown. The same data for 4 dpi as in **Fig. 1g** are shown for comparison. (**b-f**) Optogenetic manipulation of PV$^+$ neuron activity affects dendritic development of newborn neurons. Shown in (**b**) is a schematic diagram of experimental procedure. Shown in (**c**) are sample projected confocal images of immunostaining for GFP and RFP. Scale bars: 20 μm. Also shown are summaries of total dendritic length (**d**) and branch numbers (**e**). Each dot represents data from one individual neuron (**: $P < 0.01$; *: $P < 0.05$; two sample Kolmogorov–Smirnov test). Shown in (**f**) is a Sholl analysis for dendritic complexity. Values represent mean ± s.e.m. (n = 30-33 neurons; **: $P < 0.01$; two sample Kolmogorov–Smirnov test).

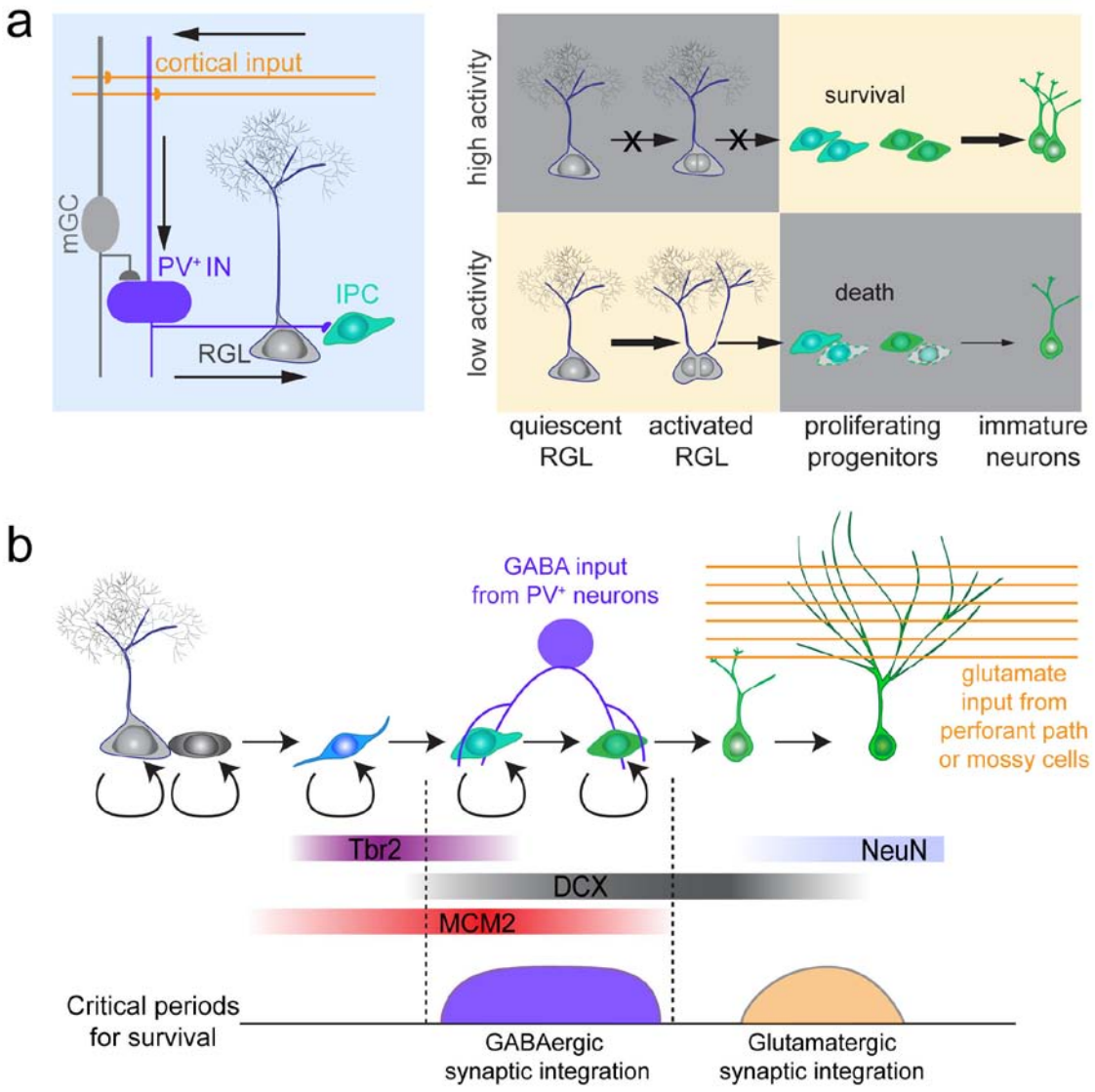

Supplementary Fig. 9. Models of activity-dependent diametric regulation of adult hippocampal neurogenesis processes and two critical periods of activity-dependent survival of newborn neuronal progeny. (**a**) Diametric regulation of two sequential proliferative processes of adult hippocampal neurogenesis by PV^+ neuron activity. Shown on the left is an illustration of the dentate circuitry where entorhinal cortical inputs activate dentate granule neurons, which in turn activate PV^+ interneurons. Shown on the right is a model of diametric regulation of quiescent neural stem cell activation and survival and maturation of their proliferative neuronal progeny: during heightened activity within dentate gyrus (top panel), activation of PV^+ neurons promotes the survival and maturation of proliferating neuronal progenitor and inhibits quiescent neural stem cell activation; conversely, when the activity in the dentate gyrus is low (bottom panel), decreased PV^+ neuron activity suppresses the survival of proliferating neuronal progenitors and simultaneously promotes expansion of the quiescent neural stem cell pool via symmetric cell division. (**b**) Two critical periods of activity-dependent regulation of progeny survival during adult hippocampal neurogenesis. The first phase occurs during GABAergic synaptic integration of proliferative newborn progeny involving PV^+ local interneurons. The second phase occurs during glutamatergic synaptic integration of post-mitotic newborn neurons via a glutamate-mediated mechanism.

Supplementary Movie 1. Close association between GFP^+ newborn progeny and $GAD67^+$Synapsin I^+ synaptic puncta in the adult dentate gyrus. Adult mice injected with onco-retroviruses to express GFP in proliferating progenitors in the adult SGZ. Shown is a surface-rendered reconstruction of a series of confocal images of the dentate gyrus (90 x 90 x 30 μm) for immunostaining of GFP (green), GAD67 (blue) and synapsin I (red) at 4 dpi.

Supplementary Movie 2. Close association between GFP^+ newborn progeny and PV^+Synapsin I^+ synaptic puncta in the adult dentate gyrus. Adult mice were injected with onco-retroviruses to express GFP in proliferating progenitors in the adult SGZ. Shown is a surface-rendered reconstruction of a series of confocal images of the dentate gyrus (90 x 90 x 30 μm) for immunostaining of GFP (green), PV (blue) and synapsin I (red) at 4 dpi.